Research Article

Nano Research
2021, 14(8): 2568–2573

ISSN 1998-0124 CN 11-5974/O4
https://doi.org/10.1007/s12274-020-3256-0

High flux photocatalytic self-cleaning nanosheet C_3N_4 membrane supported by cellulose nanofibers for dye wastewater purification

Lilong Zhang[1,2], Ge Meng[3], Guifang Fan[1], Keli Chen[2], Yulong Wu[1,4] (✉), and Jian Liu[5]

[1] *Institute of Nuclear and New Energy Technology, Tsinghua University, Beijing 100084, China*
[2] *The Key Laboratory of Bionic Engineering (Ministry of Education), Jilin University, Jilin 130012, China*
[3] *Department of Chemistry, Tsinghua University, Beijing 100084, China*
[4] *School of Chemical Engineering and Technology, Xinjiang University, Urumqi 830046, China*
[5] *College of Materials Science and Engineering, Qingdao University of Science and Technology, Qingdao 266042, China*

Received: 16 October 2020 / **Revised:** 16 November 2020 / **Accepted:** 22 November 2020

ABSTRACT

Hazardous dye substances discharged from the textile and dyestuff industries not only threaten local the surrounding ecosystems but are also hard to degraded. We report the preparation of process for a photocatalytic membrane device that can degrade dye pollution under visible light. This filtration membrane, with a well-organized multilayer structure, simultaneously achieves continuous and flow-through separation of degradation products. Cellulose nanofibers (CNFs) were used as a template for nanosheet C_3N_4 (NS C_3N_4) preparation; the performance for the photocatalytic degradation of dyes improved as the morphology changed from bulking to nanosheet. NS C_3N_4 was then attached to the surface of a prepared CNF membrane via vacuum filtration. This device exhibited high efficiency (the degradation rates of both Rhodamine B and Methylene blue both reached 96%), high flux (above 160 $L{\cdot}h^{-1}{\cdot}m^{-2}{\cdot}bar^{-1}$) and excellent stability (maintaining steady flux and high separation were maintained after 4 h). This easy-preparation, easy-scale-up, and low-cost process provides a new method of fabricating photocatalytic membrane devices for dye wastewater treatment.

KEYWORDS

high flux, nanofibers, nanosheet C_3N_4, photocatalytic membrane, dye wastewater

1 Introduction

With the rapid development of the textile and dyestuff industries, a massive quality of dye waste-water is being produced. In addition, a large amount of colored waste-water containing dyes is also released from the food, leather, and printing industries. Approximately 280,000 tons of waste-water containing dyes and textile chemicals are currently discharged annually [1]. Most dyes are not easily biodegraded, and their release into the environment poses a critical threat to the surrounding ecosystems [2]. Therefore, water pollution by dye hazardous substances has become a major concern in academia and industry. Membrane separation technology has been widely used in the treatment of dye wastewater due to its advantages of energy saving and high efficiency [3, 4]. However, when the dye waste-water goes through the membrane, the membrane pores will be filled with organic dye molecules, forming a filter cake, resulting in blockage and reduced flux. Conventional methods of cleaning process such as the use of chemicals, inevitably involve increased cost and decreased efficiency. Congestion is therefore a problem has become a bottleneck for membrane separation technologies. The photocatalytic self-cleaning method offer a solution for membrane blocking that is an alternative to conventional cleaning methods [5].

Graphitic carbon nitride (g-C_3N_4), as a metal-free photocatalysis material, has many advantages, such as being easy to prepare, inexpensive, and highly chemical stability [6, 7]. It is an ideal photocatalytic material candidate for preparing self-cleaning membrane devices. However, the development of its photocatalytic membrane devices with this material was hindered by many factors. On the one hand, because of the van der Waals forces existed between the stacked inter layers of bulking C_3N_4 [8], the conventional g-C_3N_4 usually exists in bulking form. The catalytic activity and solar energy utilization efficiency of bulking g-C_3N_4 are quite low [9]. To improve the photocatalytic efficiency, templates, such as SiO_2 and AAO, have been widely used in nanosheet-C_3N_4 (NS C_3N_4) preparation [10]. However, those strategies require template to be removed with environmentally high-risk reagents like hydrogen fluoride. Therefore, a safe, efficient, environmentally friendly, easy to operate and inexpensive method is needed for the batch production of a highly photocatalytically active two-dimensional (2D) g-C_3N_4 material for the application in the devices. On the other hand, g-C_3N_4 materials have low solubility in common solvents and cannot form stable colloidal solutions. The traditional membrane forming process such as injection, suction, and blowing process, are unsuitable for buliking C_3N_4 [11]. During compositing with other membrane supporter, the conventional bulking C_3N_4 does not easily form stable interface with supporter the materials. So, it's a challenge to prepare high-quality g-C_3N_4 membranes, and this also impede the development of applications for these materials in devices.

Address correspondence to wylong@tsinghua.edu.cn

Cellulose nanofibers (CNFs) have attracted widely attention in many fields as functional biomaterial featuring exciting properties. CNFs can link with each other to form a three-dimensional (3D) network that can be used as a template for catalyst preparation [12, 13]. Well-organized multilayer structures of CNFs membranes can be produced by self-assembly and deposition. These special structures of CNFs can offer a filtering channel to purify dye wastewater [14]. Furthermore, a network of CNFs would combine tightly with g-C_3N_4. Therefor, CNFs could not only be used as a template for nanosheet C_3N_4 (NS C_3N_4) preparation but also be a good supporter for photocatalytic membrane device. However, CNF based membranes with photocatalysis activity have rarely been reported previously.

In this study, NS C_3N_4 was prepared by using CNFs template, and a membrane foam composed consisting of CNFs and NS C_3N_4 was fabricated via the vacuum filtration method. The water pollution treatment device was designed as an alternating layered structure composed of CNFs and NS C_3N_4. With a continuous filtration experiment, a comparison was made with other types of dye wastewater treatment devices and batch-type catalytic systems.

2 Results and discussion

Figure 1(a) showed the preparation process of nanosheet C_3N_4. Liquid nitrogen was used to rapidly freeze a mixture of CNFs and melamine, allowing the CNFs to retain the 3D network structure as shown in Fig. 1(b). In this way, the formation space for C_3N_4 could be improved by the CNFs. At the same time, van der Waals forces existed in the stacked inter layers of bulking C_3N_4 would be broken. Hence, as shown in the Fig. 1(c) and Fig. S1 in the Electronic Supplementary Material (ESM), after air combustion, NS C_3N_4 was successfully exfoliated from the bulking C_3N_4. And the thickness of NS C_3N_4 is about 8 nm.

The selected area electron diffraction (SAED) pattern of NS C_3N_4 indicates a conventional crystal structure (002), as shown in Fig. 1(d). In the X-ray diffraction (XRD) patterns (Fig. 1(e)) of bulking and NS C_3N_4. The main characteristic peaks of C_3N_4 loaded at 2θ of 13° and 27.4° [15], respectively. And a wide peak loaded at 2θ of 13° belong to amorphous carbon is generated for NS C_3N_4. It means that carbonization happened during the synthesis, and because of the addition of CNFs, the NS C_3N_4 appeared more prominent. And it means that the exfoliated process only peeling the block sample into a smaller layer sample, the structural unit of the sample was not changed.

Fourier-transform infrared (FTIR) spectroscopy was also used to verify whether the morphology had any effect on the functional groups of C_3N_4. As shown in Fig. 1(f), both NS C_3N_4 and bulking C_3N_4 have similar characteristic peaks at 810, 1,170 to 1,630, and 2,180 cm^{-1}, which correspond to the triazine unit and stretching modes of the carbon nitride and the cyano groups (−C≡N), respectively [16, 17]. There is no obvious difference between NS C_3N_4 and bulking C_3N_4 in their functional groups. This result indicates that the C_3N_4 structure successfully formed during the synthesis process with CNFs addition and the change in morphology did not affect on the functional groups of the formed C_3N_4.

The CNFs template was used not only to break down the van der Waals forces existing in the bulking C_3N_4 but also to increase the surface area of NS C_3N_4. In addition, because of the carbonization process, CNFs could tightly combine with C_3N_4 so some hollows were produced in the surface of NS

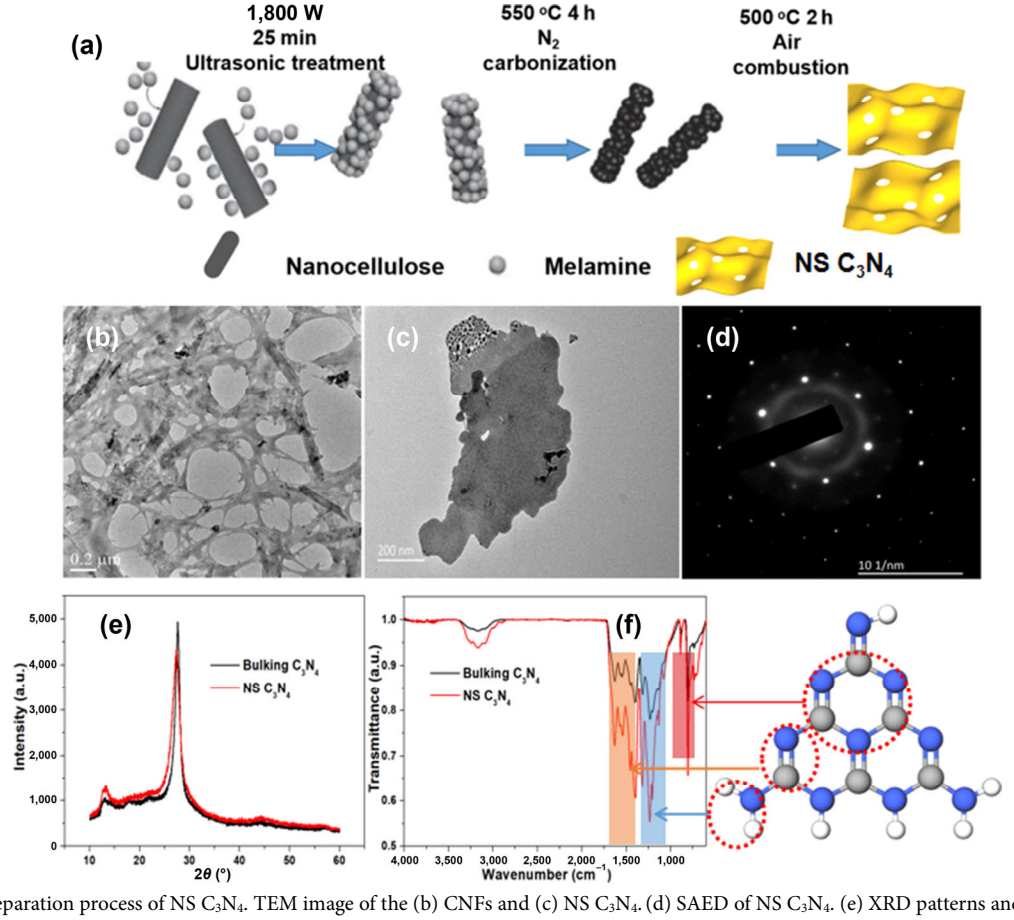

Figure 1 (a) Preparation process of NS C_3N_4. TEM image of the (b) CNFs and (c) NS C_3N_4. (d) SAED of NS C_3N_4. (e) XRD patterns and (f) FTIR spectra of the bulking C_3N_4 and NS C_3N_4.

C_3N_4 after combustion. Those surface changes in the NS C_3N_4 resulted in the Brunauer-Emmett-Teller (BET) surface area (shown in Fig. S2 in the ESM) increasing from 15.6 $m^2 \cdot g^{-1}$ of bulking C_3N_4 to 71.9 $m^2 \cdot g^{-1}$ of NS C_3N_4. Because of the higher surface area, the adsorption performance of NS C_3N_4 (26.4%) is clearly higher than that of bulking C_3N_4 (6.52%) as shown in Fig. S3 in the ESM. With the morphology modification of C_3N_4, the degradation efficiency for Methylene blue (MB) and rhodamine B (RhB) significantly increased. As shown in the Fig. 2(c), the photocatalytic kinetic constant of the NS C_3N_4 for MB (0.0336 min^{-1}) is about 3 times greater than that of bulking C_3N_4 (0.0121 min^{-1}). During the degradation process, the dye molecules were first adsorbed on the C_3N_4 surface and then degraded. Therefore, the higher degradation efficiency resulted from the better adsorption as well as from increased photocatalytic activity.

The optical absorption properties of semiconductor materials can be detected by UV–vis diffuse reflectance spectroscopy (UV–vis DRS). As can be seen in Fig. 2(a), similar peaks appear in the spectra NS C_3N_4 and the bulking C_3N_4 powder. Relative to those of the bulk C_3N_4 powder, the peaks for the NS C_3N_4 sample have 0.16 eV shifts to high binding energy, which suggested the expansion of the band gap (Fig. 2(b)). The absorption edge of C_3N_4 was at about 457 nm, assigned to a band gap of 2.6 eV, which is consistent with the reported values in the literature [18]. When the layers were stripped from the bulk by using CNFs as a template during the preparation process, the electronic structure changed and the band gap broadened [19].

Further surface analysis was carried out by X-ray photoelectron spectroscopy (XPS) to determined the surface C, N states and the chemical composition of C_3N_4. The XPS survey spectrum (Fig. 3) mainly reveals two elements (C and N). Two main peaks concentrated at binding energies of 284.7 and 288.1 eV were observed in the C 1s spectrum. The two electrons binding energy corresponds to the surface adsorbed carbon. The peaks respectively represent the sp^2-hybridized carbon atoms in N=C–N_2 and the carbon atoms in C–N of carbon. And as shown in Figs. 3(a2) and 3(b2), the NS C_3N_4 contains more in N=C–N_2 carbon atoms which means more edge defect

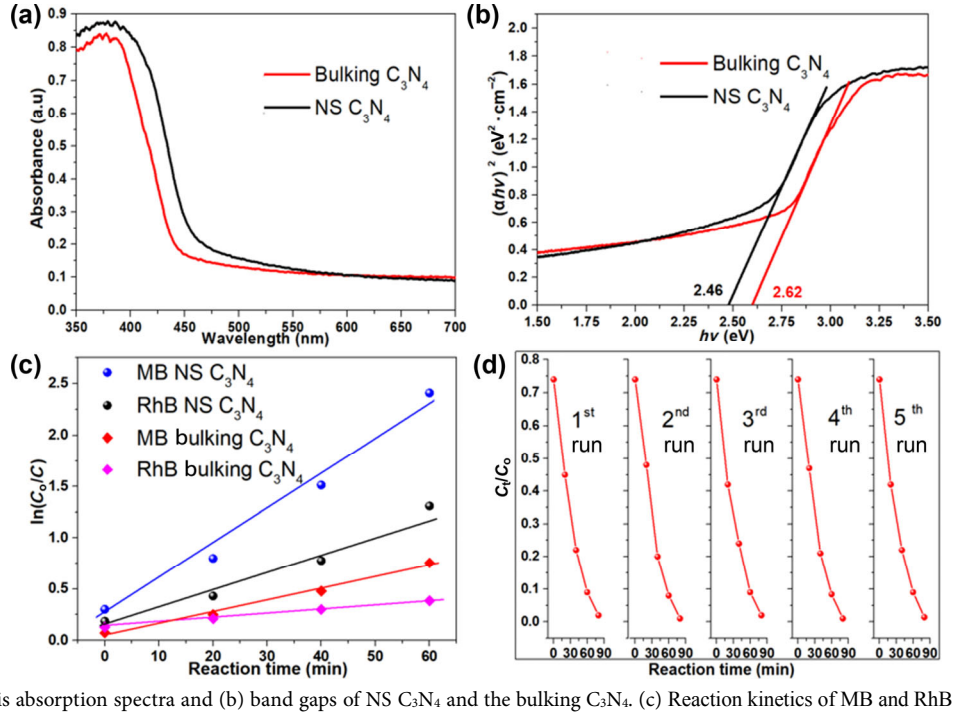

Figure 2 (a) UV–vis absorption spectra and (b) band gaps of NS C_3N_4 and the bulking C_3N_4. (c) Reaction kinetics of MB and RhB photocatalysis by NS C_3N_4 and the bulking C_3N_4. (d) MB photo-degradation cycle runs of NS C_3N_4

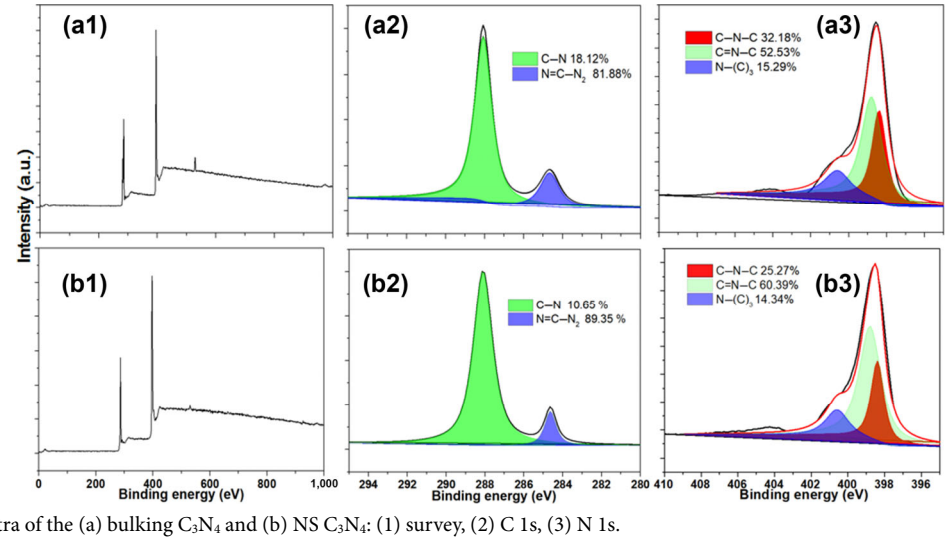

Figure 3 XPS spectra of the (a) bulking C_3N_4 and (b) NS C_3N_4: (1) survey, (2) C 1s, (3) N 1s.

formed. By peak-differentiating and imitating, the N 1s spectrum of NS C_3N_4 can be divided into three main peaks, which can be assigned to nitrogen atoms in different groups. The characteristic peaks are located at 396.7 eV, which can be assigned to sp^2 nitrogen atoms at 399.1 eV in triazine rings, assigned to the amino functional groups with a hydrogen atom (C–N–C) 402.2 eV assigned to p-excitations [20, 21]. The XPS spectra confirmed the formation of triazine units in the NS C_3N_4, which also agree with the result of FTIR spectroscopy. In contrast to the bulk C_3N_4, NS C_3N_4 shows a larger area ratio (89.35%) of the C=N–C peak. This indicates that more triazine ring units contained in the NS C_3N_4.

The inside structure and external surface of the membranes were observed via scanning electron microscopy (SEM). These CNF membranes show an ordered multilayer structure (a 10 μm thick membrane as an example is shown in Fig. 4a(1)). The multilayer structure consisting of CNFs and pores on the surface offer passages that allow water molecules to pass at a high rate [22], whereas dye molecules are rejected. The uniform pores (approximately 20 nm) are formed by regular tentacled microwires densely distributed on the surface of CNFs membrane. The tentacled microwires on the surface can tightly combine with NS C_3N_4 through the "gecko" effect (see Fig. 4(a3)), which can produce high adhesion forces [23]. Figure 4(a3) clearly shows the tentacled microwire structure of the CNFs. This kind of microstructure can tightly bond with NS C_3N_4 and form a stable structure. Therefore, the enhanced force between the CNFs and NS C_3N_4 improves the mechanical strength of the CNF/NS C_3N_4 composite membrane.

Because of the different formation processes, the adulterated and coverage membranes exhibit different structural characteristics. As shown in Fig. S4 in the ESM, although the adulterated membranes have the original multilayer structure, NS C_3N_4 fills the gap between the layers. NS C_3N_4 is uniformly distributed in the membrane, which can be seen in the cross-sectional SEM image. However, because of the layer-by-layer structure, the coverage style membrane maintains the original appearance of the CNFs. As shown in Fig. S5 in the ESM, NS C_3N_4 stacks together, and the NS C_3N_4 layers have some microscopic channels that could offer a pathway for water flow. Based on elemental distribution analysis, this membrane has a composite layer between the NS C_3N_4 and CNFs. The elemental nitrogen content exhibits a gradient decrease in this area as shown in Fig. 4(b2)). The composite layer is a combination of the upper and lower layers. It is structurally closely related to the structure of the CNFs.

For photocatalytic devices, in addition to their activity and degradation efficiency, stability is another crucial issue. As displayed in Fig. 5, the degradation of RhB and MB can reach 96% after photocatalytic device filtering. At the beginning of the photocatalytic reaction, the flux is approximately 220 $L{\cdot}h^{-1}{\cdot}m^{-2}{\cdot}bar^{-1}$, which is higher than that of commercial film. With increasing treatment time, the flux decreases to 210 $L{\cdot}h^{-1}{\cdot}m^{-2}{\cdot}bar^{-1}$. After 4 h, only an approximately 5% loss occurs in the flux, while the rejection rate remains above 95%. Therefore, this photocatalytic device exhibits high mechanical stability and high efficiency in dye degradation and maintains the same catalytic performance and good integrity.

In comparison with the results of previously reported membranes [23–25], which have included catalytic nanoparticles directly blended inside of the membrane support and on the surface of the conventional membrane, the membrane in this work exhibits exceptional performance (Fig. 5). The special structure of the membrane makes a big difference. On the one hand, with CNFs as the supports of the membrane, as shown in Fig. 4, a layer-by-layer structure with some microscopic channels is formed by combining nanofiber self-assembly. This highly ordered multilayer structure could offer a pathway for water flow [26]. This kind of multilayer structure can enhance the flux of water through the membranes with similar diameters and thicknesses [27]. On the other hand, similar to graphene oxide (GO), NS C_3N_4 can be assembled into nano channeled membranes which were widely used for water purification because of good separation performance [28]. The spacing between the artificial nanopore in the NS C_3N_4 and the partially peeled edge defect provides nanoscale channels for water transport [29, 30]. Compared with conventional commercial membranes, the g-C_3N_4 has a better performance in water flux with 29 $L{\cdot}h^{-1}{\cdot}m^{-2}{\cdot}bar^{-1}$ and a rejection rate of 87% for 3 nm molecules [31]. When these two materials combined, as shown in Fig. 4, the tentacled microwires on the nanofibers membrane surface can tightly grasp the NS C_3N_4. The combination of CNFs and NS C_3N_4 in the coverage area makes the membrane stable and attached without disruption of the nanoscale channels for

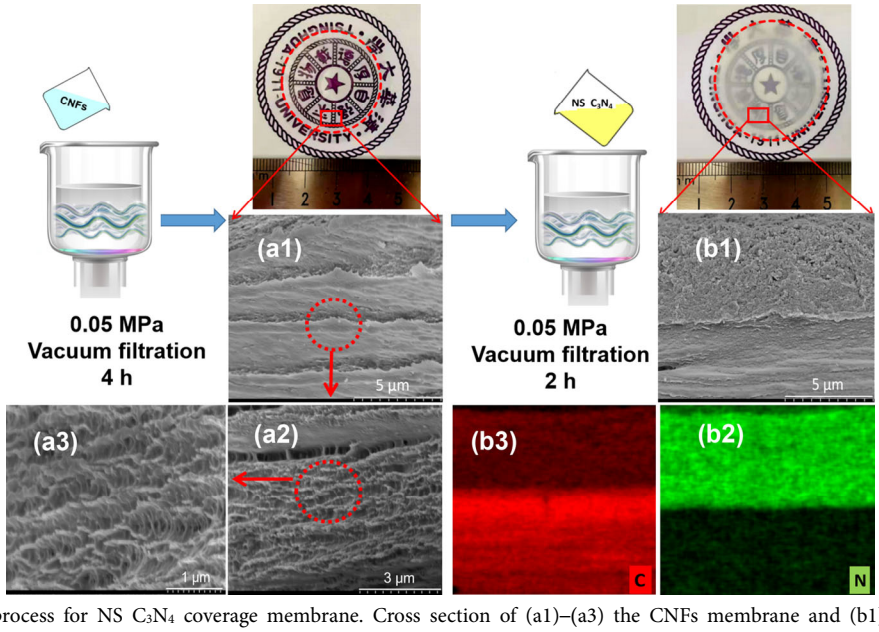

Figure 4 Preparation process for NS C_3N_4 coverage membrane. Cross section of (a1)–(a3) the CNFs membrane and (b1)) the NS C_3N_4 coverage membrane. Distribution of (b2) nitrogen and the (b3) carbon elements in the NS C_3N_4 coverage membrane.

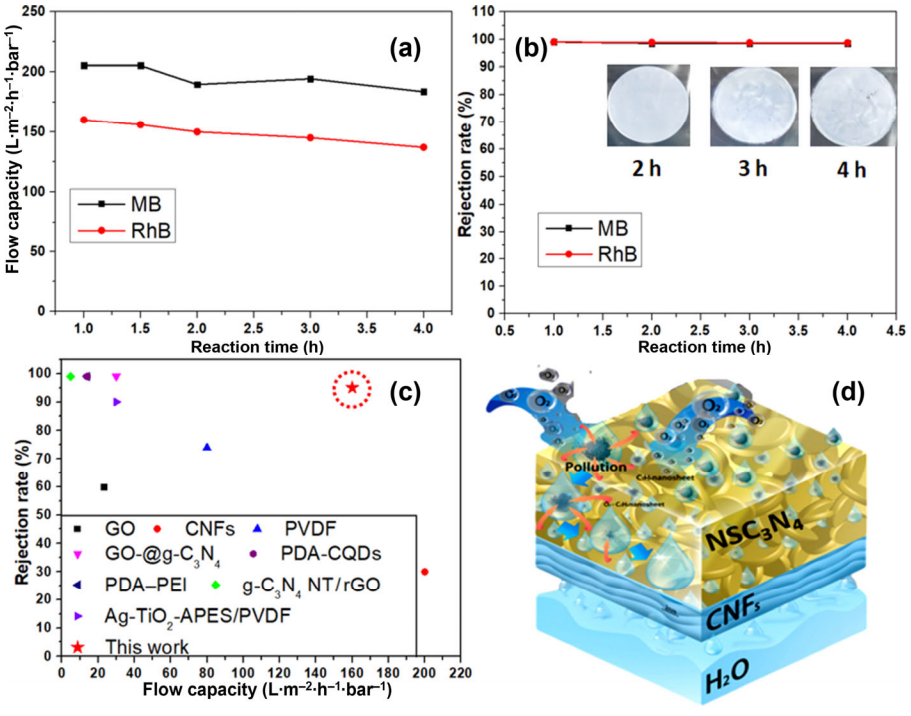

Figure 5 (a) The flow capacity and (b) rejection rate at different times (the inset image shows the surface change of the membrane). (c) Performance comparison with previous reported membranes for the separation of dyes waste water, and (d) schematic description of the degradation process for dye wastewater.

water transport. Therefore, good water penetration and high rejection are observed.

The proposed mechanism of photocatalytic degradation for dyes over NS C_3N_4 under visible light irradiation is shown in Fig. 5(d). When visible light illuminates on the surface of the NS C_3N_4, electrons and holes are generated by light and attempt to recombine on the surface of C_3N_4 [32, 33]. For NS C_3N_4, because of the morphology modification, the reactive contact area is higher than that of bulking C_3N_4, which results in an increase in the transmission efficiency of the photogenerated electrons (e^-) and holes (h^+) [34, 35]. The generated e^- can react with O_2 on the surface of C_3N_4, reducing it to the superoxide radical anion O_2^-. The dye molecules are degraded by the photogenerated h^+ and O_2^- [36]. Therefore, NS C_3N_4 can offer more reaction surfaces for the O_2 and the dye molecules, so more O_2^- anions participate in the dye degradation reactions, which results in an increase in the photocatalytic performance.

3 Conclusion

CNFs were first used as templates for nanosheet C_3N_4 (NS C_3N_4) preparation. NS C_3N_4 exhibits excellent photocatalytic activity relative to that of bulking C_3N_4 powder. High flux photocatalytic self-cleaning NS C_3N_4 membranes supported by CNFs were prepared by simple suction filtration. This type of continuous photocatalytic reaction device not only shows fast water penetration (above 160 $L{\cdot}h^{-1}{\cdot}m^{-2}{\cdot}bar^{-1}$) but also exhibits high efficiency (above 96%) in the degradation of dyes (RhB and MB) and good catalytic stability (continuous and reliable operation for more than 4 h).

This work has provided a new method for NS C_3N_4 preparation and may extend the C_3N_4 membrane device applications in dye water treatment.

Acknowledgements

This study was financially supported by the National Key R&D Program of China (No. 2018YFC1902101), the National Natural Science Foundation of China (Nos. 21908127, 21838006, and 21776159), the project supported by the Foundation (No. KF201810) of Key Laboratory of Pulp and Paper Science and Technology of Ministry of Education/Shandong Province of China and Opening Project of the Key Laboratory of Bionic Engineering (Ministry of Education), Jilin University.

Electronic Supplementary Material: Supplementary material (experimental procedures, computational details, supplementary figures and tables, characterization of isolated product) is available in the online version of this article at https://doi.org/10.1007/s12274-020-3156-0.

References

[1] Bora, L. V.; Mewada, R. K. Visible/solar light active photocatalysts for organic effluent treatment: Fundamentals, mechanisms and parametric review. *Renew. Sust. Energ. Rev.* **2017**, *76*, 1393–1421.

[2] Liu, P. T.; Liu, Y. G.; Ye, W. C.; Ma, J.; Gao, D. Q. Flower-like N-doped MoS_2 for photocatalytic degradation of RhB by visible light irradiation. *Nanotechnology* **2016**, *27*, 225403.

[3] Saha, N.; Rahman, M. S.; Ahmed, M. B.; Zhou, J. L.; Ngo, H. H.; Guo, W. S. Industrial metal pollution in water and probabilistic assessment of human health risk. *J. Environ. Manage.* **2017**, *185*, 70–78.

[4] Tabassum, S.; Zhang, Y. J.; Zhang, Z. J. An integrated method for palm oil mill effluent (POME) treatment for achieving zero liquid discharge—A pilot study. *J. Clean. Prod.* **2015**, *95*, 148–155.

[5] Wang, Y.; Wang, X. C.; Antonietti, M. Polymeric graphitic carbon nitride as a heterogeneous organocatalyst: From photochemistry to multipurpose catalysis to sustainable chemistry. *Angew. Chem., Int. Ed.* **2012**, *51*, 68–89.

[6] Wang, J. L.; Xu, L. J. Advanced oxidation processes for wastewater treatment: Formation of hydroxyl radical and application. *Crit. Rev. Environ. Sci. Technol.* **2012**, *42*, 251–325.

[7] Anwer, H.; Mahmood, A.; Lee, J.; Kim, K. H.; Park, J. W.; Yip, A. C. K. Photocatalysts for degradation of dyes in industrial effluents: Opportunities and challenges. *Nano. Res.* **2019**, *12*, 955–972.

[8] Guo, Y. R.; Liu, Q.; Li, Z. H.; Zhang, Z. G.; Fang, X. M. Enhanced photocatalytic hydrogen evolution performance of mesoporous graphitic carbon nitride Co-doped with potassium and iodine. *Appl. Catal. B Environ.* **2018**, *221*, 362–370.

[9] Wang, X. S.; Zhou, C.; Shi, R.; Liu, Q. Q.; Waterhouse, G. I. N.; Wu, L. Z.; Tung, C. H.; Zhang, T. R. Supramolecular precursor strategy for the synthesis of holey graphitic carbon nitride nanotubes with enhanced photocatalytic hydrogen evolution performance. *Nano. Res*. **2019**, *12*, 2385–2389.

[10] Zhao, Z. W.; Sun, Y. J.; Dong, F. Graphitic carbon nitride based nanocomposites: A review. *Nanoscale* **2015**, *7*, 15–37.

[11] Hao, Q.; Jia, G. H.; Wei, W.; Vinu, A.; Wang, Y.; Arandiyan, H.; Ni, B. J. Graphitic carbon nitride with different dimensionalities for energy and environmental applications. *Nano. Res*. **2018**, *13*, 18–37.

[12] Klemm, P.; Kramer, F.; Moritz, S.; Lindström, T.; Ankerfors, M.; Gray, D.; Dorris, A. Nanocelluloses: A new family of nature-based materials. *Angew. Chem., Int. Ed*. **2011**, *50*, 5438–5466.

[13] Yang, W. G.; Feng, Y. H.; He, H. Z.; Yang, Z. T. Environmentally-friendly extraction of cellulose nanofibers from steam-explosion pretreated sugar beet pulp. *Materials* **2018**, *11*, 1160.

[14] Lee, J.; Lim, M.; Yoon, J.; Kim, M. S.; Choi, B.; Kim, D. M.; Kim, D. H.; Park, I.; Choi, S. J. Transparent, flexible strain sensor based on a solution-processed carbon nanotube network. *ACS Appl. Mater. Interfaces* **2017**, *9*, 26279 − 26285.

[15] Liu, J.; Wang, H. Q.; Antonietti, M. Graphitic carbon nitride "reloaded": Emerging applications beyond (photo)catalysis. *Chem. Soc. Rev*. **2016**, *45*, 2308–2326.

[16] Zhang, H. B.; An, P. F.; Zhou, W.; Guan, B. Y.; Zhang, P.; Dong, J. C.; Lou, X. W. Dynamic traction of lattice-confined platinum atoms into mesoporous carbon matrix for hydrogen evolution reaction. *Sci. Adv*. **2018**, *4*, eaao6657.

[17] Zheng, Y.; Jiao, Y.; Zhu, Y. H.; Cai, Q. R.; Vasileff, A.; Li, L. H.; Han, Y.; Chen, Y.; Qiao, S. Z. Molecule-level g-C_3N_4 coordinated transition metals as a new class of electrocatalysts for oxygen electrode reactions. *J. Am. Chem. Soc*. **2017**, *139*, 3336–3339.

[18] Li, H. T.; Li, N.; Wang, M.; Zhao, B. P.; Long, F. Synthesis of novel and stable g-C_3N_4-Bi_2Wo_6 hybrid nanocomposites and their enhanced photocatalytic activity under visible light irradiation. *R. Soc. Open Sci*. **2018**, *5*, 171419.

[19] Xu, J.; Zhang, L. W.; Shi, R.; Zhu, Y. F. Chemical exfoliation of graphitic carbon nitride for efficient heterogeneous photocatalysis. *J. Mater. Chem. A* **2013**, *1*, 14766–14772.

[20] Zheng, Y.; Lin, L. H.; Wang, B.; Wang, X. C. Graphitic carbon nitride polymers toward sustainable photoredox catalysis. *Angew. Chem., Int. Ed*. **2015**, *54*, 12868–12884.

[21] Qi, K. Z.; Xie, Y. B.; Wang, R. D.; Liu, S. Y.; Zhao, Z. Electroless plating Ni-P cocatalyst decorated g-C_3N_4 with enhanced photocatalytic water splitting for H_2 generation. *Appl. Surf. Sci*. **2019**, *466*, 847–853.

[22] Lai, T. M.; Du, Z. W.; Chen, Y. G. Abnormally large and small adhesion forces between plasma-treated silicon surfaces studied on AFM. *J. Adhesion* **2019**, 1–23.

[23] Li, R.; Ren, Y. L.; Zhao, P. X.; Wang, J.; Liu, J. D.; Zhang, Y. T. Graphitic carbon nitride (g-C_3N_4) nanosheets functionalized composite membrane with self-cleaning and antibacterial performance. *J. Hazard. Mater*. **2019**, *365*, 606–614.

[24] Shao, D. D.; Yang, W. J.; Xiao, H. F.; Wang, Z. Y.; Zhou, C.; Cao, X. L.; Sun, S. P. Self-cleaning nanofiltration membranes by coordinated regulation of carbon quantum dots and polydopamine. *ACS Appl. Mater. Interfaces* **2020**, *12*, 580–590.

[25] Wei, Y. B.; Zhu, Y. X.; Jiang, Y. J. Photocatalytic self-cleaning carbon nitride nanotube intercalated reduced graphene oxide membranes for enhanced water purification. *Chem. Eng. J*. **2019**, *356*, 915–925.

[26] Ling, S. J.; Qin, Z.; Huang, W. W.; Cao, S. F.; Kaplan, D. L.; Buehler, M. J. Design and function of biomimetic multilayer water purification membranes. *Sci. Adv*. **2017**, *3*, e1601939.

[27] Ling, S. J.; Jin, K.; Kaplan, D. L.; Buehler, M. J. Ultrathin free-standing *Bombyx mori* silk nanofibril membranes. *Nano Lett*. **2016**, *16*, 3795–3800.

[28] Nair, R. R.; Wu, H. A.; Jayaram, P. N.; Grigorieva, I. V.; Geim, A. K. Unimpeded permeation of water through helium-leak-tight graphene-based membranes. *Science* **2012**, *335*, 442–444.

[29] Surwade, S. P.; Smirnov, S. N.; Vlassiouk, I. V.; Unocic, R. R.; Veith, G. M.; Dai, S.; Mahurin, S. M. Water desalination using nanoporous single-layer graphene. *Nat. Nanotechnol*. **2015**, *10*, 459–464.

[30] Zhou, L.; Tan, Y. L.; Wang, J. Y.; Xu, W. C.; Yuan, Y.; Cai, W. S.; Zhu, S. N.; Zhu, J. 3D self-assembly of aluminium nanoparticles for plasmon-enhanced solar desalination. *Nat. Photonics* **2016**, *10*, 393–398.

[31] Wang, Y. J.; Li, L. B.; Wei, Y. Y.; Xue, J.; Chen, H.; Ding, L.; Caro, J.; Wang, H. H. Water transport with ultralow friction through partially exfoliated g-C_3N_4 nanosheet membranes with self-supporting spacers. *Angew. Chem., Int. Ed*. **2017**, *56*, 8974–8980.

[32] Li, F.; Yu, Z. X.; Shi, H.; Yang, Q. B.; Chen, Q.; Pan, Y.; Zeng, G. Y.; Yan, L. A mussel-inspired method to fabricate reduced graphene oxide/g-C_3N_4 composites membranes for catalytic decomposition and oil-in-water emulsion separation. *Chem. Eng. J*. **2017**, *322*, 33–45.

[33] Liu, Q. X.; Ai, L. H.; Jiang, J. Mxene-derived TiO_2@C/g-C_3N_4 heterojunctions for highly efficient nitrogen photofixation. *J. Mater. Chem. A* **2018**, *6*, 4102–4110.

[34] Yan, P. C.; She, X. J.; Zhu, X. W.; Xu, L.; Qian, J. C.; Xia, J. X.; Zhang, J. M.; Xu, H.; Li, H. N.; Li, H. M. Efficient photocatalytic hydrogen evolution by engineering amino groups into ultrathin 2D graphitic carbon nitride. *Appl. Surf. Sci*. **2020**, *507*, 145085.

[35] Tian, N.; Huang, H. W.; Du, X.; Dong, F.; Zhang, Y. H. Rational nanostructure design of graphitic carbon nitride for photocatalytic applications. *J. Mater. Chem. A* **2019**, *7*, 11584–11612.

[36] Gan, X. R.; Lei, D. Y.; Ye, R. Q.; Zhao, H. M.; Wong, K. Y. Transition metal dichalcogenide-based mixed-dimensional heterostructures for visible-light-driven photocatalysis: Dimensionality and interface engineering. *Nano. Res*. **2020**, DOI: 10.1007/s12274-020-2955-x.